COBEM 2023 27TH INTERNATIONAL CONGRESS OF MECHANICAL ENGENEERING

ABCM Brazilian Society of Mechanical Sciences and Engineering
27th ABCM International Congress of Mechanical Engineering
December 04-08, 2023, Florianópolis-SC, Brazil

COBEM2023-2131
PARAMETERIZATION OF LASER CLADDING PROCESS WITH WC AND H13 IN CONSIDERING DILUTION ASPECTS

Paulo Paiva Oliveira Leite Dyer
Silvelene Alessandra Silva
Instituto de Estudos Avançados EFO/IEAv, Instituto Nacional de Pesquisas Espaciais INPE/LAS
paulo_dyer@yahoo.com, lenisoni@uol.com.br

Andersan dos Santos Paula
Rafael Ramos
Instituto Militar de Engenharia
andersan@ime.eb.br

Maria Margareth da Silva
Getúlio de Vasconcelos
Instituto Tecnológico de Aeronautica, Instituto de Estudos Avançados EFO/IEAv
maria.margareth@gp.ita.br, getuliovas@gmail.com

Abstract. *Laser clad automated processing becomes more and more widespread in manufacturing industry. Meeting an increasingly demanding for cost reduction to purchasing and line or contract activities stoppage. As well, the reduction of worn parts disposal. However, according to literature, these processes aren't systematized. In this way, this paper aimed a production of process chart, determining laser cladding parameters for a better efficiency. Using H13 and WC powders as cladding under structural steel substrates, based on optimal cladding morphology. For this, a 1500W Ytterbium fiber laser was used. With beam diameter of 6 mm, coupled to a Yaskawa Motoman robot arm. The process chart shown a dilution of 39 % with a clad angle of 152° optimum. With parameters of velocity of scanning of 5 mm/s, 85% of laser power efficiency and powder feed rate of 4.4 g/min. Thus, improving micro hardness (MHV) properties than starting materials. Concurrently, the algorithm implemented on the robotic arm, produced a virtual scenario when transferred to software RoboDK. With this it was possible to modify the laser track to suit other application scenarios. Thus, this methodology development was able to optimize automated cladding processes. Besides producing a mirror-virtual interface, contributing to its continuous improvements.*

Keywords: *Laser cladding, robotic arm, laser dilution, clad angle, parametrization 4.0 manufacturing clad industry*

1. INTRODUCTION

Laser cladding had a considering advances in coating techniques along the last 20 years. Initially in laboratorial way but, rapidity integrating manufacture chains, improving tools and parts surface properties, improving they wear and toughness resistance (Wang et al., 2022).

Currently, with the 4.0 Industry rising, the processes become more robust and precise. Including compact and higher power lasers beams; imbued with a broad of frequencies, spots sizes and beam profiling types (Lotzmann et al., 2017; Wang et al., 2022). Likewise, according to Kaierle et al. (2012), the pre-deposition or direct cladding powder deposition also needs to be in constant upgraded, attending the highest efficiency and industrial velocity demands; such as aspersive injection and extreme high speed laser application (EHLA) techniques.

In this context, as Yong et al. (2023) stated, EHLA systems have a kind of "transparency commitment" with the cladding, i.e., with the laser beam "seeing" the substrate surface without much powder obstruction. Consequently, it is expected an energy transference to the cladding and substrate, enough to provide a satisfactory metallurgical bonding between them. Where this distributive ratio is in the order of 60-80% and 20% to substrate and cladding, respectively; differently to Laser-based directed energy deposition (DED-LB) systems, standing around 80/20% (Svetlizky et al., 2022). Thus, EHLA becomes more attractive to manufacturing environment, allowing a coating quality assurance, in face of an optimized process imbued of powder efficiency and highest "v_s" scanning speeds (Yong et al., 2023).

Furthermore, the demand for handling advances brings more precise and high pay-load capacity equipment; as the robotic arms (Torims, 2013). Jumping from optical focused XY variation marking heads or computational numerical control (CNC) tables; using, in mainly, low intensity lasers with small spots; to up 6-axes degrees of freedom robust

machines (Ya et al., 2016). With this, automating, and thus, optimizing even more the clad process; since, as highlighted by Torims (2013), the cladding begins in computational processing way, with a programming development form.

Nevertheless, the misplacing of studies, aggregating the cladding process advances is noted; with few researches pointing check-list and boundary conditions for clad parameters determination, in mirroring to computational environment way; whereas EHLA and pre-deposition processes, in face of metallic and matrices metallic ceramic powders. In order to determine an assurance parameter for v_s, laser power "P" and powder feeder rate "μ" or pre-deposited powder thickness "e" (Wang et al., 2023). According to Pellizzari et al. (2022), the visual macro measurements (by optical microscopy OM), such as dilution ratio (D); determined by Goodarzi et al. (2015); and clad angle (α) act as a qualitative boundary condition, in view of a process chart containing a several cross sections samples; in face of predictive optimized EHLA configuration way, such as the focus match of feeder powder nozzle and laser beam and correct focal distance of laser to the substrate adjustment. Wirth and Wegener (2018), in turn, underline the virtual environment prediction parameters, optimizing the boundary conditions constraints. In this way, they highlights the tracking trajectory (by line segments), robot flange axis normalization, temperature control (by deposition or irradiation passes controlling) and EHLA track thickness control; in addition, the reproducibility in other material types conditions assurance. In order to attend the optimized cladding conditions, assuring the metallurgical bonding quality this paper aims parametric system organization to laser beam parameter definition. To this end, this paper aimed a parametrization of clad process, throughout a several of analyses; imbued with a computational simulation scenario coupled to the practical steps.

2. METHODOLOGICAL DEVELOPMENT

The relationship between cladding parameters; according to literature; were used as a parameter definition basis. Then, experiments set-up were re-set, aiming the clad process optimization; and then, new experiments were performed. The samples were analyzed by optical microscopy (OM), creating a "process chart"; evaluating dilution (D) and clad angle (α) parameters. Likewise, scanning electron microscopy (SEM), electron dispersive spectroscopy (EDS) and microhardness Vickers test (MHV) complemented this framework of tests. Simultaneously, the robot arm configuration and laboratory spatial position were transferred to the virtual environment. With this, a virtual "working place" was built, determining a computational modeling environment; well re-applied for other parameters for other projects.

2.1 Materials, Equipment and Software

Were used a SAE 4340 and stainless-steel substrates (SS 360L); here generically defined as "structural steel". Since, the objective doesn't analyze a specific steel alloy. H13 and WC powders were used as coatings, whose particle size properties, microstructures and composition are presented in Figure 1 and Table 1. Furthermore, the list of equipment and software used for cladding, material characterization and computational modeling is presented in Table 2.

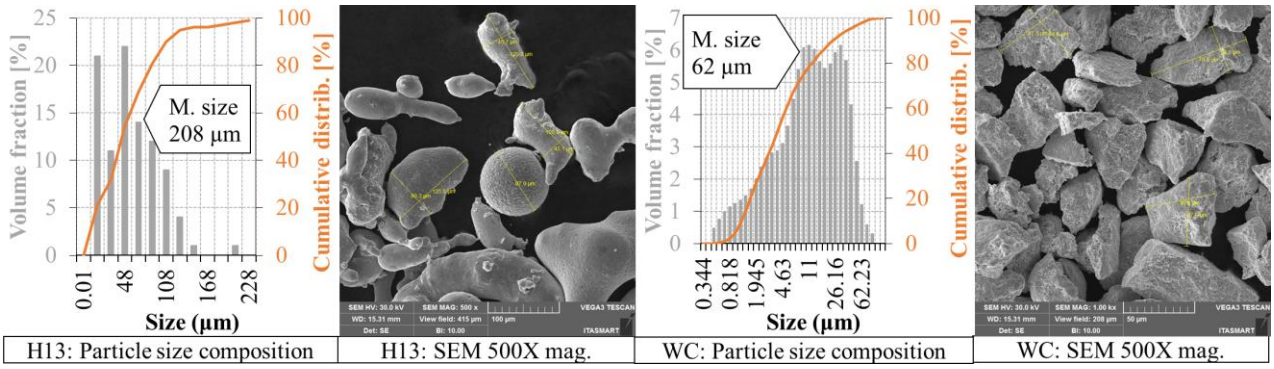

Figure 1. Cladding powders granulometric composition and microstructures.

Table 1. H13, WC and substrate materials chemical composition.

Materials		**Elements (W%)**									
	C	Co	Cr	Fe	O	Mo	Mn	Ni	Si	V	W
H13	-	-	4.74	92.37		1.48	-	-	0.54	0.87	-
WC	8.30	9.50	4.20	-	3.50	-	-	-	-	-	74.60
SAE 4340	0.36	-	0.79	95.80		0.22	0.64	1.70	-	-	-
Stainless-steel 316L	0.03	-	17.17	71.1		-	1.90	8.700	0.50	-	-

Table 2. Equipment and its uses.

Equipment	**Use**	**Equipment**	**Use**
Aropol 2V polishing	Metallographic Preparation	Software RoboDK	Robot programing
Buehler SimpliMet 3000	Metallographic Preparation	Soft. TopSolid, AutoCAD	Modeling
YLR-1500-MM-WC IPG: Ytterbium fiber laser with 1500 W of maximum power "*P*", top-hat profiling, "b_d" of 6 mm, wavelength of 1.07 µm, supply power of 220 V and M^2 of 1.1	Laser Cladding	IPG Chiller system	Laser clad support
AT-1210 Thermach with capacity of 3.6 liters	Feeding H13 to EHLA	STC-HD203DV/32" LCD	Visual monitoring
COCACO comb gauge	Setting the pre-deposited WC layer	Zeiss microscope	OM analysis
Yaskawa GP25: payload of 25 kg and length of 1500 mm	Laser loading for track scanning	FM-700 micro durometer	MHV test
50 liters argon gas tank	Shielding and powder transport	Tescan Mira3	SEM/EDS analyst

2.2 Methodology

The cladding parameters were deduced using; as the basis; the parameters arrangement of beam intensity and energy density equations (Decker, 1995; Vilar 1999; Keist and Palmer, 2016). Thus, the fixed; as the beam diameter or spot "b_d" and laser power "*P*"; and variable as scan speed "v_s", powder feeder rate "μ" and power efficiency "*E*" parameters were regrouped obtaining Eq. (1). And then, the "*k*" term was kept constant, with input data from Pellizzari's et al. (2022) best results (α = 149.08°, *D* = 7.5%) and IPG laser fixed parameters. With this, were defined central parameters of: v_s, μ and *E* for the EHLA (H13) and pre-deposition (WC) processes. Where, for WC; as the μ = 0; the conversion of Eq. (2) was used, whose considered beam spot area and "ρ" WC density for WC powder thickness "*e*" definition.

$$k = [EP][(60v_s)(b_d\mu)]^{-1} \quad (1)$$

$$e = 66.67[\mu][\pi\rho v_s b_d]^{-1} \quad (2)$$

Where the "*k*" term was kept constant, in order to ratio the optimal Pellizzari's et al. (2022) parameters to the IPG laser conditions; obtaining the input parameters for Eq. (1) and Eq. (2) balancing, as Table 3 shown. In addition, this table shows the shielding conditions "s_g" and transport gas "s_t" flow.

Table 3. definition of parameters for balancing Eq. (1) and Eq. (2).

Variables	**Unit**	**Parameters**		
		Comparative: Pellizzari et al. (2022)	Fixed (WC/IPG Laser)	Obtained
s_g	l/min	5.00	5.00	-
s_t	l/min	5.00	5.00	-
v_s	mm/seg	17.00	-	6.00
E	%	100.00	-	70.00
P	W	1800.00	1500.00	-
μ	g/min	10.00	-	8.00
b_d	mm	3.00	6.00	-
e	µm	-	-	302.00
ρ	g/mm³	-	0.02	-
k	W.min²/mm²g	0.06	-	0.06

Next, these "central" v_s, *E*, μ and *e* obtained parameters were extended for maximum and minimum values, observing the laboratory experiences. With this, were defined all experiment parameters; before and after optimization; as Table 4 shown. Pointing that, this table also contemplates experiments terminology as "*TR-1* to *26*"; indicating the cladding proprieties as a single straight track. With a single layer passage with powder for EHLA and only irradiation for pre-deposited powder. The cladding optimization, in other hand, was applied initially to the both methods; sequentially, was applied as individually and personalized way to the methods of EHLA an pre-deposited, as the Figure 2 flow chart shown.

Table 4. Experiments performing parameters.

Tracks (H13)	v_s	E	μ	Optim.	Tracks (WC)	v_s	E	e	Optim.
TK-1	3 (min.)	70	7.2 (max.)	Before	*TK-14*	3 (min)	85	500 (max.)	Before
TK-2	4	70	7.2	Before	*TK-15*	5	75	500	Before
TK-3	5	70	6 (central)	Before	*TK-16*	6 (central)	75	500	Before
TK-4	5	70	7.2	Before	*TK-17*	11 (max)	30	500	Before
TK-5	5	75	7.2	Before	*TK-18*	5	40	0-300	Before
TK-6	5	80	7.2	Before	*TK-19*	10	40	0-300	Before
TK-7	6 (central)	70	6	Before	*TK-20*	15	40	0-300	Before
TK-8	11 (max.)	70	6	Before	*TK-21*	5	60	0-300	Before
TK-9	5	82	3.69	After	*TK-22*	4	60	0-300	Before
TK-10	5	85	4.4	After	*TK-23*	4	70	0-300	Before
TK-11	5	82	4.65	After	*TK-24*	4	50	200	After
TK-12	5	85	7.2	After	*TK-25*	4	60	200	After
TK-13	8	82	4.65	After	*TK-26*	4	70	200	After

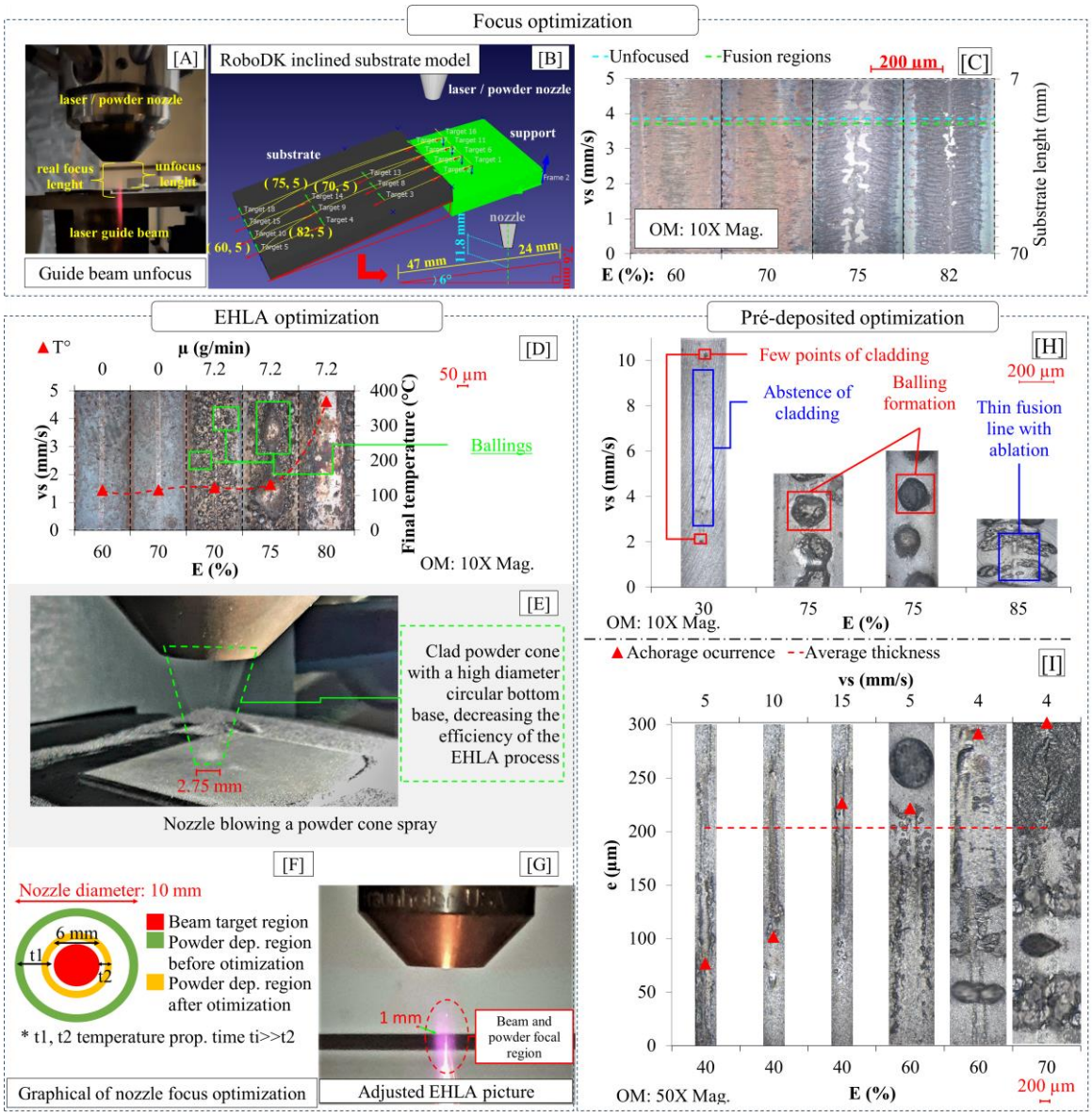

Figure 2. Clad optimization process flowchart.

As the Figure 2 shown, firstly the laser beam focal length to the substrate surface was adjusted. Since, the STC-HD203DV camera focus didn't coincided with beam focus, as illustrated in Figure 2[A]. For this purpose, an inclined

structural steel substrate (angle = 6°) was irradiated with (E, v_s) = (60, 5), (70, 5), (75, 5) and (82, 5) pairs of parameters, as shown in Figure 2[B]. Thus, the new focus was calculated: from 11.8 to 12.6mm; by triangles similarity, considering the best tracks morphology (as fusion occurrence), as shown in OM micrographs of Figure 2[C]. Furthermore, during the EHLA was measured a high substrate temperature level, with "balling" formation in high E level, as the graph of Figure 2[D] shown; evidencing a powder nozzle miss adjustment (Figure 2[E]). Thus, the nozzle factory position was reconfigured, reducing the area from the laser target to the nozzle deposition region, as Figure 2[F] graphs explain. With this, was reached the expected EHLA energy ratio distribution of: 20/80% to substrate/clad powder; according to Li et al. (2019); as illustrated by Figure 2[G]. Notwithstanding, the *TK-14* to *17* tracks (e = 500 µm max, uniform) also showed shortcomings. With, balling or no clad anchoring occurrence, as shown in the OM micrographs in Figure 2[H]. With that, *TK-18* to *23* tracks were performed in a variable thickness deposition from zero to e = 300 µm defined by Eq. (2); determining an optimum thickness of 200 µm, from *TK-24* to *26* tracks analysis, as shown in the graph of Figure 2[I].

Before the laboratory experiments, the modeling environment was built throughout two fronts: programming parameters set up and working place digitalization, as Figure 3 flowchart shown.

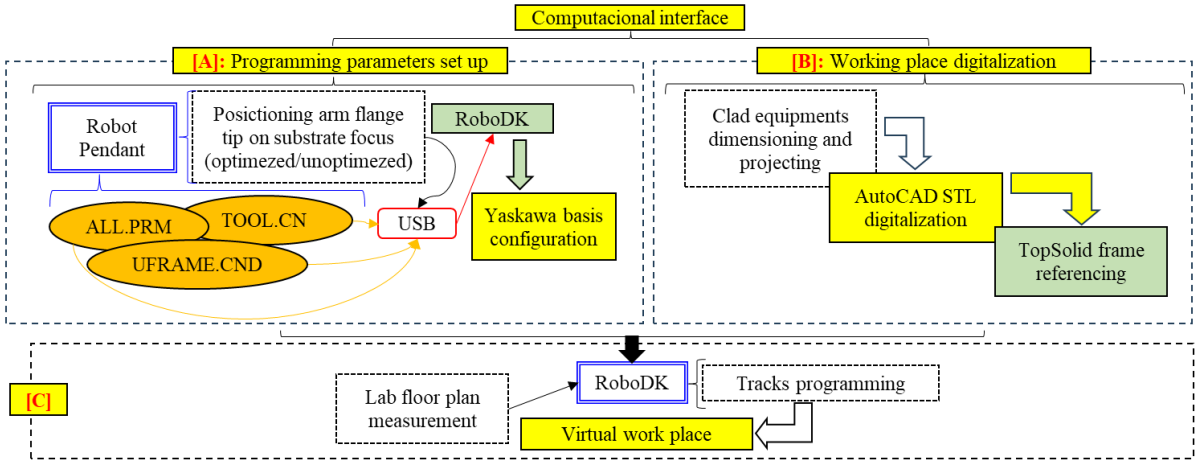

Figure 3. Flowchart of computational interface procedures methods.

As Figure 3 shown, for programming front, initially were loaded to RoboDK the configuration archives from robot joystick (pendant). These files: "ALL.PRM", "TOOL.CND" and "UFRAME" are essential for Euler angles to pulses coordinates converting; and robot arm tool configuration. Since, the Yaskawa arm operates with Euler angles, in addition, the "standard tool" reference is located at the arm flange tip; requiring these adjustments for programing. Likewise, flange tip position, under the substrate focus, were transferred to RoboDK; correlating the coordinates of model with experiment set-up spatial position, with the Figure 3[A] highlighting this front. At the digitization front, in turn, Table 2 equipment were dimensioned and converted into digital solids or "STL" using AutoCAD. Being referenced by positioning frames definition in TopSolid, as detailed in "[B]". Then, using the flange tip coordinates and the laboratory floor plan measurement, all reference frames were defined at RoboDK. With this, the room real dimensions with Yaskawa basis and equipment STL were overlapped. Thus, a virtual workplace were composited, as detail the "[C]" step of flowchart. From this modeling, the 1-track programing were generated in RoboDK; enabling the parameters (v_s, E and μ) modifications. With real/virtual movements correlativity assurance; avoiding collisions or equipment and samples damaging.

3. RESULTS AND DISCUSSION

Through the OM of cross sections, were measured: clad area "A_c", molten area "A_m", clad width "W", clad height "H_c" and melt depth "H_m"; using the AutoCad digitalization. Then, inserted in Oliveira et al. (2005) Eq. (3) and (4).

$$D = A_m(A_C + A_m)^{-1} \tag{3}$$

$$\propto = 180 - 2\tan^{-1}([2H_c][W]^{-1}) \tag{4}$$

Where, the relationship between cladding areas and heights; as graph of Figure 4 shown; represent the best condition for coating parameters, as stated by Pellizzari et al. (2022). Thus, the process chart of Figure 5 was obtained, together with the α and D, as Table 5 shown, for all cladded tracks (*TK-1* to *TK-13* and *TK-24* to *TK-26*); including the WC pre-deposited tracks 24-26, considering the thickness "e" with powder rate "μ" in the chart.

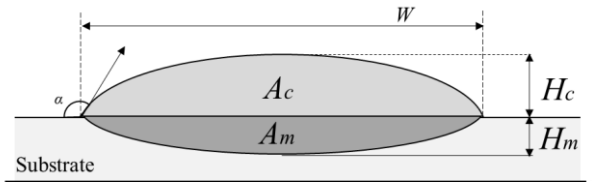

Figure 4. Graphical representation of the cladding variables.

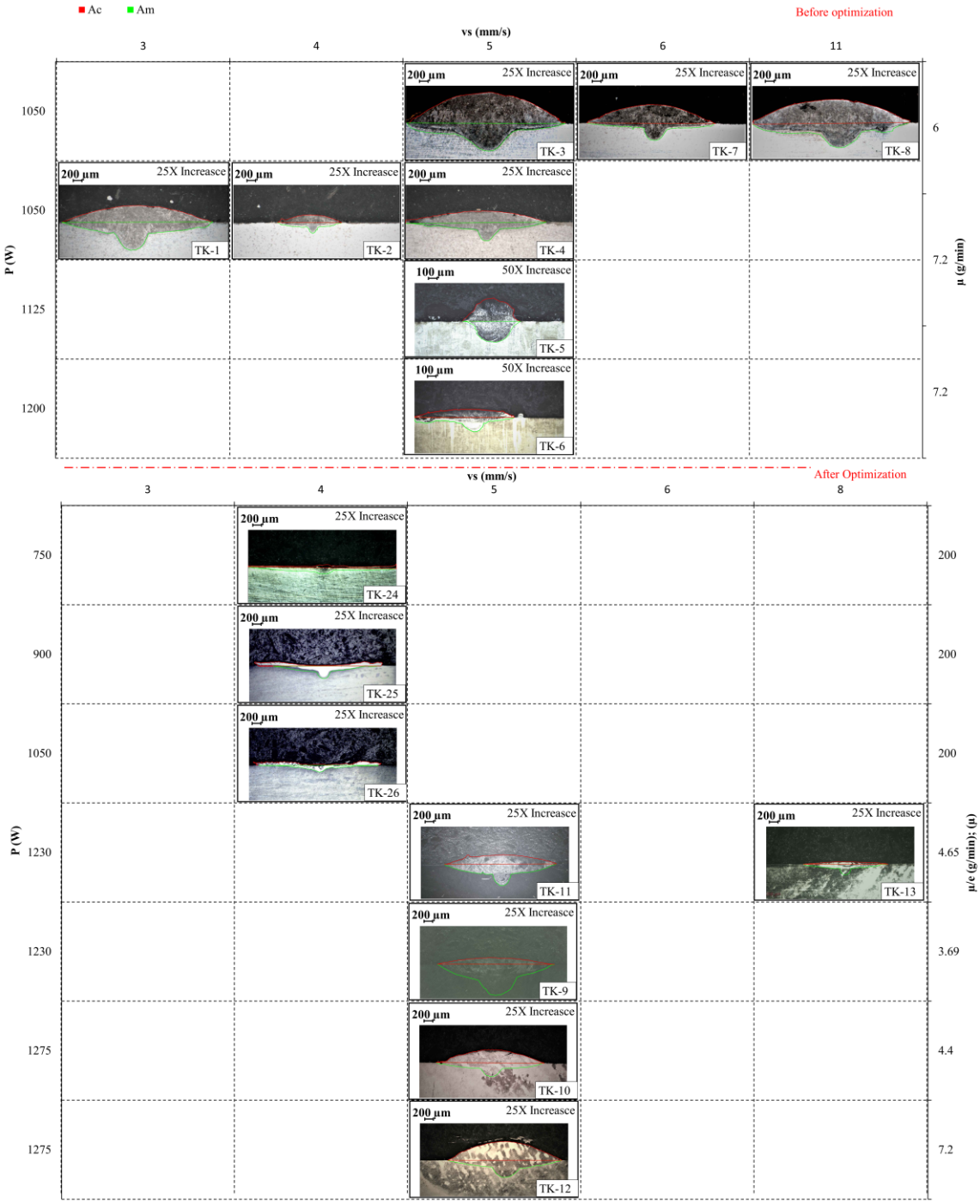

Figure 5. Dilution and clad angle process chart of coated tracks.

Table 5. Cladding properties according to the process chart diagram.

Tracks	**Dilution Variables**						
	W mm	*Hc* mm	*Hm* mm	*Ac* mm²	*Am* mm²	*D* %	*α* grade
Criteria [1]:						8-14	149-162
TK-1	3.24	0.36	0.62	0.75	0.77	50.61	154.89
TK-2	1.49	0.18	0.25	0.18	0.14	44.11	152.10
TK-3	3.55	0.71	0.63	1.60	0.93	36.75	136.36
TK-4	3.06	0.25	0.42	0.54	0.37	40.82	161.34
TK-5	0.63	0.26	0.23	0.10	0.08	44.72	101.25
TK-6	2.25	0.18	0.33	0.30	0.28	48.40	161.65
TK-7	3.02	0.45	0.40	0.86	0.37	30.23	146.98
TK-8	3.49	0.55	0.53	1.27	0.83	39.45	144.90
TK-9	2.76	0.15	0.73	0.52	1.82	77.76	167.38
TK-10	2.46	0.31	0.30	0.90	0.58	39.18	152.08
TK-11	2.50	0.20	0.50	0.69	0.97	58.41	161.47
TK-12	2.66	0.44	0.39	1.49	0.83	35.72	143.48
TK-13	1.94	0.05	0.24	0.13	0.32	70.21	174.04
TK-24	6.89	0.19	0.23	0.54	0.82	60.64	173.70
TK-25	5.55	0.18	0.56	0.54	0.80	59.82	172.55
TK-26	5.44	0.16	0.30	0.56	0.42	42.58	173.43
[1]	Pellizzari et al. (2022)						

These results shown no one H13/structural-steel track achieving the Peliazzi's et al. (2022) criteria for *D*; with dilutions in order of >>14%. According to Oliveira et al. (2005) and Goodarzi et al. (2015), this panorama is can be explained by the same composition of clad and substrate; practically a steel under another steel. This similarity increase the miscibility between them during the fusion; increasing the substrate diffusion zone depth (Goodarzi et al., 2015). However, the tracks morphology presented a consistent variation, as a clad parameters function; according to literature (Pellizzari et al., 2022; Wang et al., 2022). With this, the *α* Pellizzari's et al. (2022) criteria meets the *TK-1* and *TK-2* (before optimization); with the *TK-10* (after optimization) imbued with best results; indicating a well cladding occurrence with these parameters. Likewise, the MHV test shown a 40% of increase, comparing to the other tracks MHV average, as Figure 6 graph shown. Demonstrating that the Eq. (1) defined parameters; or besides nearby; were effective for H13 cladding, with the set-up optimization improving this clad quality. The WC/structural-steel samples, on the other hand, showed a thin layer coat, as evidenced by Jardim (2020). Nonetheless, unlike that was observed by this author, a single layer track deposition didn't make assurance for a well cladding formation; observing clearing ablative evidence, with the clad penetrating the substrate with a far morphology for *α* Pellizzari et al. (2022) criteria. In addition, the MHV test shown results WC hardness outside of typically expected according to literature (Callister Jr. and Rethwisch, 2014); evidencing a ceramic particle escaping from the metal matrix of cladding. As Jardim (2020) studied, this fault could be solved by overlaying new layers; since, the *TK-24* to *26* thin cladding presents an average thickness of 100 µm.

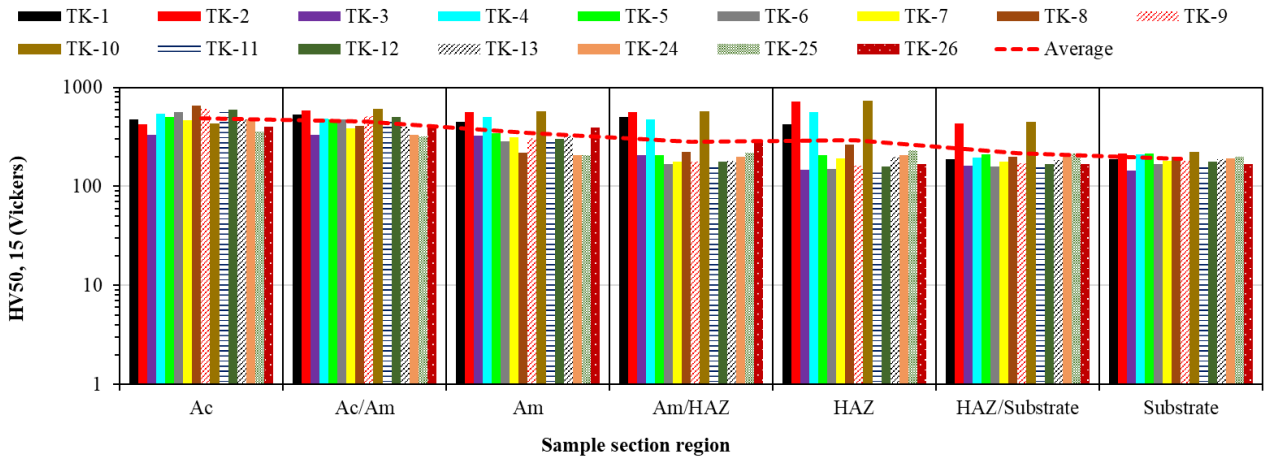

Where: Ac and Am are the cladding lenght regions with heat affectec zone (HAZ) and substrate regions. With these respective interfaces "/" regions

Figure 6. MHV test results for coated tracks.

Therefore, the (E, v_s, μ) = (5, 85, 4.4) parameters of *TK-10*; after set-up optimization; produced the best α value and highest HV50, 15 = 434 for coated region. In fact, as SEM, EDS mapping and EDS shown in Figure 7 and Table 6, were observed a few occurrences of pores, ablative effects and balling. Likewise, Figure 7[A] (SEM) shown dendritic structures occurrence, evidencing the metallurgical bonding between cladding and substrate. In addition, Figure 7[B] (EDS mapping), demonstrates a homogeneous elements distribution of among materials; being confirmed by Figure 7[C] EDS by regions (Spectrum 1 to 7); whose elemental composition were correlated by Table 6.

From this prospectus discusses that the correlation between fixed and variable parameters; using the clad morphology as boundary conditions; with set-up optimization, possibilities the definition of the: E, v_s and μ parameters in more assertively way; considering the EHLA technique for metallic powders (such as H13). For pre-deposited WC, however, this parameterization sequence didn't produce a well cladding; in a first view. Although, these results shown a further possibility for experiments; as a sequence of WC layers overlapping deposition due to the clad thin thickness formation.

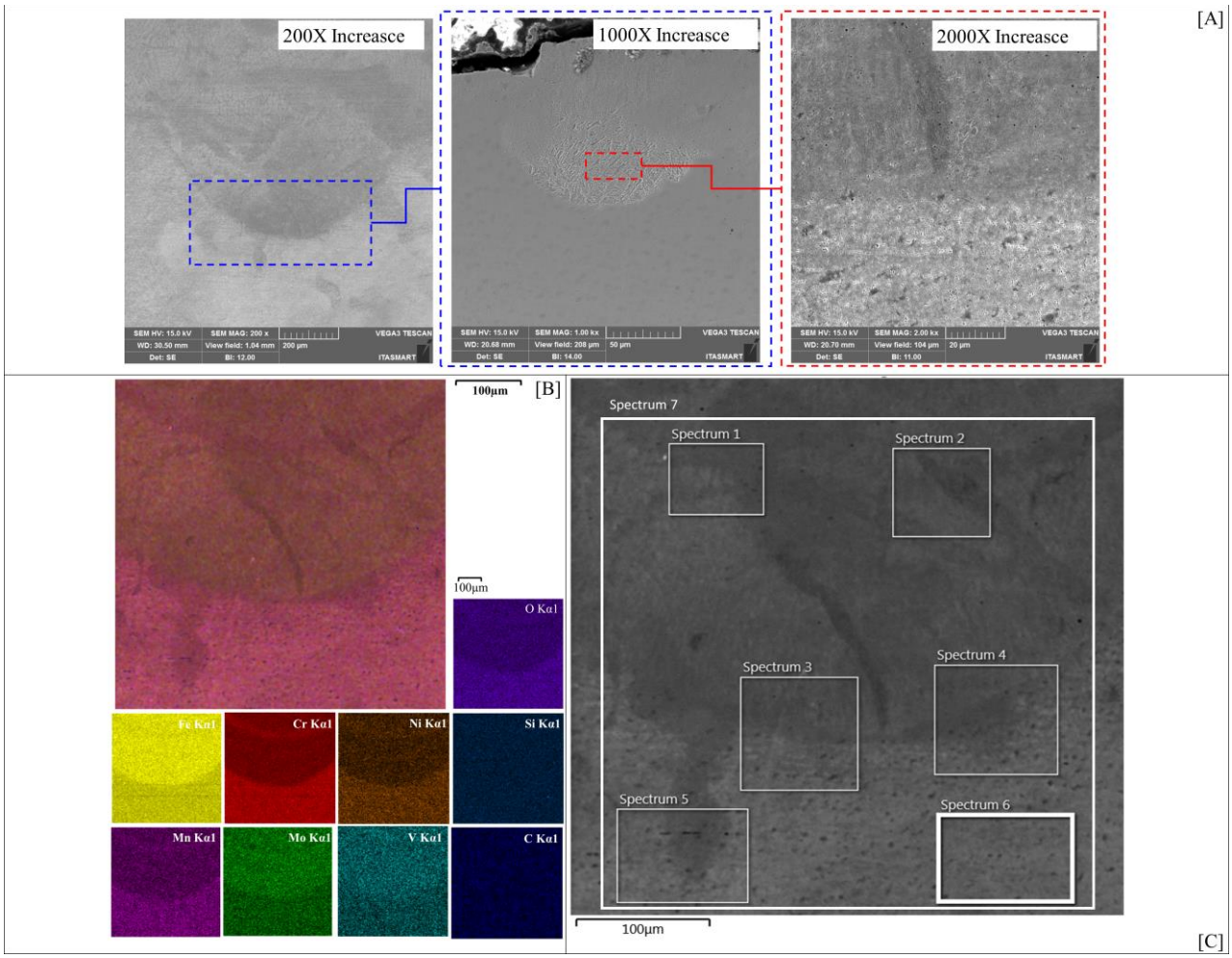

Figure 7. SEM and EDS mapping of *TK-10* track.

Table 6. Chemical composition of *TK-10*, according to Figure 7[C] regions spectrum.

Elements	**EDS area (Spectrum)**						
	1	2	3	4	5	6	7
C	3.40	3.00	3.40	3.20	3.60	3.40	3.20
Cr	12.40	12.40	14.90	15.60	17.70	18.20	14.20
Fe	75.10	76.40	71.90	70.50	66.90	67.00	73.00
Mn	0.70	0.80	1.00	1.10	1.20	1.00	0.90
Mo	1.00	0.50	0.30	0.50	0.30	0.30	0.90
Ni	5.00	4.80	6.00	6.20	7.30	7.40	5.60
O	1.70	1.10	1.90	2.20	2.40	2.30	1.80
Si	0.50	0.40	0.40	0.40	0.60	0.50	0.40
V	0.30	0.50	0.20	0.30	-	-	0.20

The computational interface, in the other hand, was crucial to experiments planning. In that, the programming tracks were intruded in the virtual work place, imbedding the Table 2 digitized equipment. With they inserted on each floor plan laboratory room location; according it's individual reference frames, as the graphic scheme of Figure 8 shown.

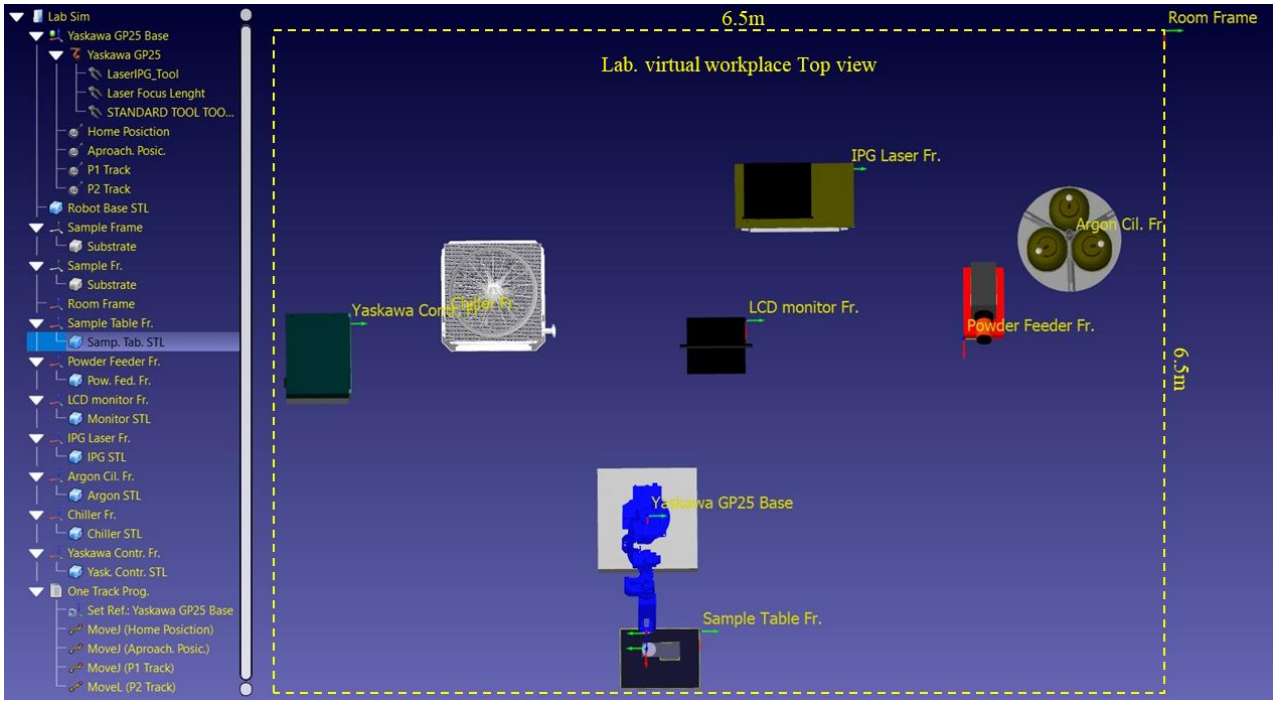

Figure 8. Virtual workplace top view.

This interface possibilities a standardized experiments execution; avoiding collisions and other accidents. In addition, the virtual workplace integrate the equipment function, in order to predict they role during the cladding process. With this, was possible to change parameters, experiments reproducibility and adaptability in a more efficient way; as Figure 9[A] graphic details. Where, initially the "one track prog" (Figure 9[B]) programs were inputted in Yaskawa arm pendant; with the robot CPU cabinet processing them. Next, the "E" parameters were set in the IPG laser controller. Then, during the cladding, the chiller performed the laser cooling while, the argon gas cylinder supplied the "s_g" shield gas to sample table (Figures 9[C, D]). Likewise, along the EHLA experiments, the "s_t" gas were supplied to the powder feeder; carrying the H13 powder to the laser beam. In parallel, the LCD monitor captured and displayed real time top view images.

With this, the computational interface followed the experiments, producing a virtual model. Thus, integrating virtual and experimental parameters; creating a methodology to standardize and determine assertive cladding parameters.

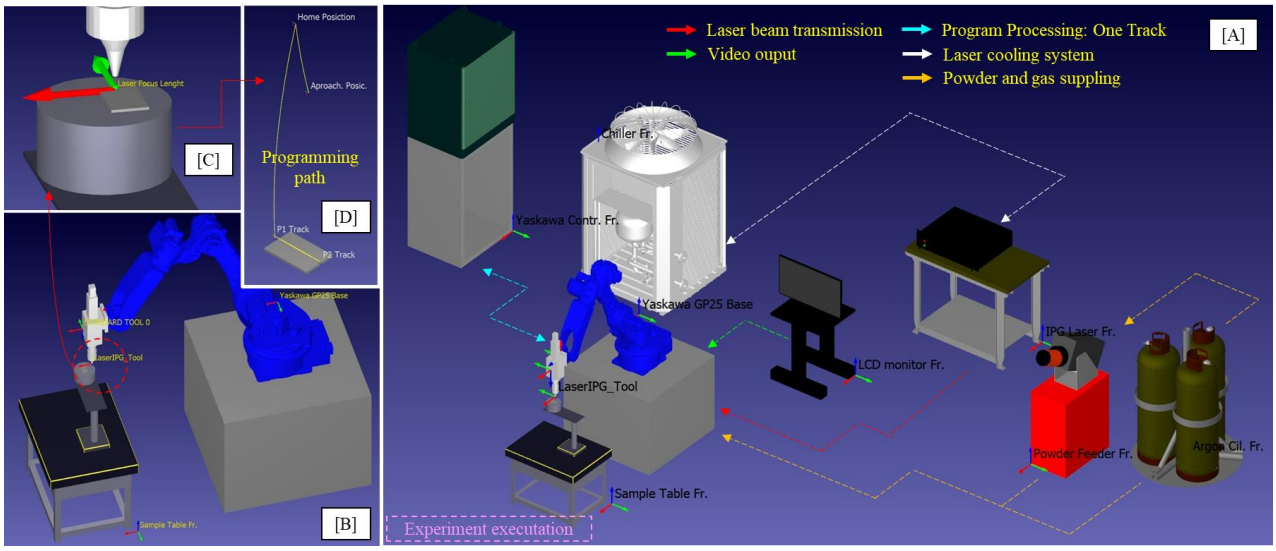

Figure 9. Perspective view of workplace detailing the equipment function and its experiment role.

4. CONCLUSION

As presented in this paper, concluded that the correlation between fixed and variable parameters; considering cladding morphology; determine assertively parameters for laser cladding. Furthermore, a parallel virtual scenario contributes to the control, safety and process efficiency; producing a methodology to standardize the laser cladding processes, making them more assertive and efficient. A primordial requisite in currently industrial scenario, since the dynamic and 4.0 industrial chain needs become more and more, new and efficient process.

5. ACKNOWLEDGEMENTS

We thank to Instituto de Estudos Avançados Instituto Militar de Engenharia, Instituto Tecnológico de Aeronáutica, and Instituto Nacional de Estudos Espaciais for support team and facilities. This work was funded by CNPq, under the grant: 405624/2022-0; CAPES, under the grant: 88887.285953/2018-00, and FINEP, under the grant: 25670-SUB-1.

6. REFERENCES

Callister Jr., W. D., Rethwisch, D. G., 2014, *Materials Science and Engineering An Introduction*. Willey, Danver.

Decker, F. .J., 1995. “Beam distributions beyond RMS”. In *Proceedings of the AIP Conference Proceedings 1995*.

Goodarzi, D. M., Pekkarinen, J., Salminenet, A., 2015, Effect of process parameters in laser cladding on substrate melted areas and the substrate melted shape, Journal of Laser Applications, Vol. 27, pp. 1387.

Jardim, V.R., 2020. *Characterization of tungsten carbide coating deposited by laser fusion on titanium alloy Ti 6Al-4V*. Ph.D. thesis, Graduate Program in Applied Physics and Mathematics, Aeronautical Technological Institute, São José dos Campos, Brasil.

Kaierle S., Barroi, A., Noelke, C., Hermsdorf, J., Overmeyer, L., Haferkampet, H., 2012, Review on Laser Deposition Welding: From Micro to Macro, Physics Procedia, Vol. 39, pp. 336.

Keist, J. S., Palmer, T. A., 2016, Role of geometry on properties of additively manufactured Ti-6Al-4 V structures fabricated using laser based directed energy deposition, Materials Design.

Li, L., Shen, F., Zhou, Y., Tao, W., 2019, Comparative study of stainless steel AISI 431 coatings prepared by extreme-high-speed and conventional laser cladding, Journal of Laser Applications, Vol. 31.

Lotzmann, T., Wenzel, F., Karsunkeet, U. al., Kozak, K., 2017, Industrial Laser Systems: For Industry 4.0, visualization and machine learning can be combined to enhance laser processing, Fraunhofer IWS, Dresden, Germany, https://www.sylodium.com/en/news/industrial-laser-systems-for-industry-40/2064. Accessed 18 May 2023.

Oliveira, U., OcelÍk, V., De Hosson, J. Th. M., 2005, Analysis of coaxial laser cladding processing conditions, Surface & Coatings Technology, Vol. 197, pp. 136.

Pellizzari, M., Zhao, Z., Bosetti, P., Periniet, M., 2022, Optimizing direct laser metal deposition of H13 cladding on CuBe alloy substrate, Surface & Coatings Technology, Vol. 432, pp. 128084.

Svetlizky, D., Zheng, B., Vyatskikh, A., Das, M., Susmita, B., Bandyopadhyay, A., Schoenung, J. M., Lavernia, E. J., Eliazet, N., 2022, Laser-based directed energy deposition (DED-LB) of advanced materials, Materials Science & Engineering A, Vol. 840, pp. 142967.

Torims, T., 2013, The application of laser cladding to mechanical component repair, renovation and regeneration, Chapter 32 in DAAAM International Scientific Book 2013, pp. 587-608.

Vilar, R., 1999, Laser cladding, Journal of Laser Applications, Vol. 11, pp. 346.

Wang, K., Liu, W., Hong, Y., Shakhawat Sohan, H. M., Tong, Y., Hu, Y., Zhang, M., Zhang, J., Xiang, D., Fu, H., Juet, J., al., 2023, An Overview of Technological Parameter Optimization in the Case of Laser Cladding, Coatings, Vol. 13, pp. 496.

Wang, K., Zhang, Z., Xiang, D., Ju, J., 2022, Research and Progress of Laser Cladding: Process, Materials and Applications, Coatings, Vol. 1382.

Wirth, F., Wegener, K., 2018, A physical modeling and predictive simulation of the laser cladding process, Additive Manufacturing, Vol. 2010.

Ya, W., Pathiraja, B., Liu, S., 2016, 2D modelling of clad geometry and resulting thermal cycles during laser cladding, Journal of Materials Processing Technology, Vol. 230, pp. 232.

Yong, Z., Chang, L., Jiang, S., Xie, D., Xing, F., Shen, H., Shen, L., Tianet, Z., 2023, Parameter optimization of T800 coating fabricated by EHLA based on response surface methodology, Optics & Laser Technology, Vol. 158, Part A, pp. 108837.